

Multi-Stability and Multi-Instability Phenomena in a Mathematical Model of Tumor-Immune-Virus Interactions

Raluca Eftimie · Jonathan Dushoff ·
Byram W. Bridle · Jonathan L. Bramson ·
David J.D. Earn

Received: 28 October 2010 / Accepted: 15 March 2011 / Published online: 8 April 2011
© Society for Mathematical Biology 2011

Abstract Recent advances in virology, gene therapy, and molecular and cell biology have provided insight into the mechanisms through which viruses can boost the anti-tumor immune response, or can infect and directly kill tumor cells. A recent experimental report (Bridle et al. in *Molec. Ther.* 18(8):1430–1439, 2010) showed that a sequential treatment approach that involves two viruses that carry the same tumor antigen leads to an improved anti-tumor response compared to the effect of each virus alone. In this article, we derive a mathematical model to investigate the anti-tumor effect of two viruses, and their interactions with the immune cells. We discuss the conditions necessary for permanent tumor elimination and, in this context, we stress the importance of investigating the long-term effect of non-linear interactions. In particular, we discuss multi-stability and multi-instability, two complex phenomena that can cause abrupt transitions between different states in biological and physical systems. In the context of cancer immunotherapies, the transitions between a tumor-free and a tumor-present state have so far been associated with the multi-stability phenomenon. Here, we show that multi-instability can also cause the system to switch from one state to the other. In addition, we show that the multi-stability is driven

R. Eftimie (✉) · D.J.D. Earn
Department of Mathematics and Statistics, McMaster University, Hamilton, ON L8S 4K1, Canada
e-mail: reftimie@math.mcmaster.ca

J. Dushoff
Department of Biology, McMaster University, Hamilton, ON L8S 4L8, Canada

B.W. Bridle · J.L. Bramson
Centre for Gene Therapeutics, Department of Pathology and Molecular Medicine, McMaster University, Hamilton, ON L8N 3Z5, Canada

J. Dushoff · J.L. Bramson · D.J.D. Earn
Michael G. DeGroote Institute for Infectious Disease Research, McMaster University, Hamilton, ON L8N 4L8, Canada

by the immune response, while the multi-instability is driven by the presence of the virus.

Keywords Cancer immunology · Oncolytic virus · Mathematical model · Multi-stability · Multi-instability

1 Introduction

The use of viruses to treat cancer has a long history, beginning with the anecdotal reports of spontaneous cancer remission following viral infections or viral vaccinations (Dock 1904; Bluming and Ziegler 1971; Hansen and Libnoch 1978). Despite numerous advances in virology, gene therapy and molecular and cell biology, there are still no standard anti-cancer virotherapies (although a number of viruses have been used in later stages of clinical trials in humans (Mullen and Tanabe 2002)). The main challenge for a successful therapy is to understand the delicate balance between the immune-mediated viral clearance and the anti-tumor viral efficacy (Mullen and Tanabe 2002). In particular, the two important aspects of cancer viral therapy are: (a) the direct anti-tumor effect caused by the use of replicating oncolytic viruses (i.e., viruses that infect and selectively replicate inside cancer cells), and (b) the indirect effect caused by the amplification of the anti-tumor immune response. While oncolytic viruses have tremendous potential for cancer therapy, their effect can be greatly diminished by anti-viral immune responses (Silva et al. 2010). To overcome this problem, Bridle et al. (2010) developed a sequential treatment protocol that involved the use of two viruses (a vaccine virus and an oncolytic virus) which carried the same tumor-associated antigen (human dopachrome tautomerase (hDCT)). The first virus (an adenovirus (Ad)) was used to trigger an immune response against the tumor antigen. The second virus (an oncolytic vesicular stomatitis virus (VSV)) served to boost the anti-tumor immune response, in addition to killing the tumor directly. Bridle et al. (2010) found that the secondary immune response against tumor antigens dominated the response against viral antigens. (The immune response was measured by the number of $CD8^+$ T cells that infiltrate the tumor and produce $IFN-\gamma$.) This resulted in significant viral replication and tumor destruction. On average, mice survived for 54 days following the combined effect of the two viruses, compared to a maximum of 30 days following the administration of each virus alone. Despite this improved survival rate, the majority of mice showed tumor re-growth.

In this article, we aim to investigate the interactions among the tumor cells, immune cells, and two viruses in the context of the experimental protocol of Bridle et al. (2010). Our goal is to develop a mathematical model that reproduces the experimental dynamics, and then use it to identify biological conditions that could lead to permanent elimination of cancer cells.

For the past 10–15 years, various mathematical models have been derived to investigate the delicate balance between the anti-tumor and anti-viral immune responses (Wein et al. 2003; Friedman et al. 2006; Bajzer et al. 2008; Wodarz and Komarova 2009; Biesecker et al. 2010; Wu et al. 2004; Wodarz 2001). These models range

from very simple equations describing the interaction between the infected and uninfected tumor cells (Wodarz and Komarova 2009), to more complex models that investigate the spatial dynamics of various types of tumor cells (infected, uninfected, and necrotic), immune cells and oncolytic viruses (Wein et al. 2003). In general, the models focus only on the effector immune cells, since these cells are critical for tumor elimination. However, for the dual-immunization protocol described by Bridle et al. (2010) the magnitude of the secondary effector immune response (following the oncolytic virus (VSV)) is dependent on the magnitude of the memory immune response (following the vaccine virus (Ad)). For this reason, in this paper, we model not only the effector $CD8^+$ T cells but also the memory $CD8^+$ T cells elicited by the Ad vaccine. To describe the interactions of these cells with the tumor and the virus particles, we use a two-compartment model. The two compartments, namely the lymphoid compartment (where the memory T cells reside and antigen presentation takes place), and the peripheral compartment (where the tumor is located), can account for the delay in the tumor-immune dynamics. The model investigated in this paper falls into the general class of non-spatial ODE models reviewed by Eftimie et al. (2010).

The non-linear interactions among the tumor cells, viruses, and immune cells are expected to give rise to complex behaviors that could explain the permanent elimination (or lack thereof) of tumor cells. As an example, nonlinear tumor-immune interactions were shown to give rise to primary and secondary bifurcations (Byrne et al. 2004) and bi-stability (Lefever and Horsthemke 1979; Bunimovich-Mendrazitsky et al. 2007; Lejeune et al. 2008). *Bi-stability* or more general *multi-stability*, is an important feature of many biological systems that can operate in two (or more) distinct modes. Examples of bi-stable and multi-stable behaviors can be found in a variety of biological systems, from the molecular pathways that regulate cell kinetics (EiBing et al. 2004; Pomerening 2008; Reth and Brummer 2004; Chang et al. 2006; Angeli et al. 2004), to the macroscopic behavior of insects (Buhl et al. 2006), or the temporal patterns of infectious disease epidemics (Schwartz and Smith 1983; Earn et al. 2000). Investigating the mechanisms that could cause bi-stable or multi-stable behaviors can provide useful information regarding the abrupt transitions between different states. In cancer immunology, the interest is in the biological mechanisms that could explain sudden transitions from a tumor-free to a tumor-present state, and vice versa (Lefever and Horsthemke 1979; Kirschner and Panetta 1998; Bunimovich-Mendrazitsky et al. 2007; Cappuccio et al. 2007; Lejeune et al. 2008). Examples of such mechanisms are the rate at which the immunotherapeutic agent is introduced into the system (Bunimovich-Mendrazitsky et al. 2007; Kirschner and Panetta 1998), the tumor antigenicity (Kirschner and Panetta 1998), or the ratio of tumor proliferation and tumor elimination rates (Lejeune et al. 2008).

Another complex behavior that could lead to abrupt changes in the dynamics of a system is *multi-instability*. This phenomenon has been studied quite intensively in physical (Schwartz and Carr 1999) or epidemiological (Billings and Schwartz 2002; Choisy et al. 2006) systems. However, multi-instability has not received much attention in models for cancer immunotherapy. As opposed to multi-stability, multi-instability (which is characterized by several equilibria, cycles or more complex lim-

iting states being unstable at the same time) can lead to unexpected outcomes. In epidemiology, for example, chaotic patterns of disease outbreaks could be stimulated by heteroclinic connections resulting from bi-instability (Billings and Schwartz 2002; Choisy et al. 2006). Similar chaotic behavior has been observed in a delayed differential model for virus-immune interactions (Canabarro et al. 2004). In this article, we show that the multi-instability phenomenon could lead to a transition from a tumor-present to a tumor-free state (and vice versa). This transition is the result of a global homoclinic bifurcation (see Perko 2000 for a general discussion of such bifurcations). Here, we identify this bifurcation graphically, and discuss its implications for the outcome of the anti-cancer viral therapy. Also, we show that the multi-instability phenomenon is related to the persistence of the oncolytic virus, while the multi-stability phenomenon is related to the anti-tumor immune response. For the parameters investigated in this model, we have not detected chaotic behavior.

We begin in Sect. 2 by deriving the mathematical model. In Sect. 3, we discuss the local behavior of the system and the conditions that ensure the stability of the steady states. In Sect. 4, we discuss the short-time and long-time behavior of the system. In particular, we focus on the conditions that can lead to multi-stability and multi-instability. We also discuss the effect of these two phenomena on the transition from a tumor-present to a tumor-free state. Finally, in Sect. 5, we summarize and discuss the biological implications of the multi-stability and multi-instability phenomena for the improvement of cancer immunotherapies.

2 Model Description

The tumor-immune-virus interactions depend on the migration of cells and viral particles into the solid tumor, as well as on the tumor architecture (Blohm et al. 2006; Breitbach et al. 2007). Mathematically, these interactions could be modeled with the help of spatial models based on partial differential equations (Araujo and McElwain 2004). However, since these models can become quite complicated, as a first step in the modeling process we do not model this spatial component explicitly and use instead compartmental ODE models. To account for the delay in the tumor-immune interactions induced by the spatial component, we introduce two compartments: the lymphoid compartment (where the immune cells get activated and proliferate) and the peripheral compartment (where the tumor is localized) (see Fig. 1).

To model the anti-tumor and anti-viral immune responses, we focus on the changes in the tumor size (denoted by x), the size of the immune response (denoted by y), and the magnitude of the viral infection (denoted by v) following the injection of two viruses: an oncolytic virus (the vesicular stomatitis virus (VSV)) and a vaccine virus (the adenovirus (Ad)). To measure the effect of the oncolytic virus on the tumor cells, we model separately the time evolution of uninfected (x_u) and infected (x_i) tumor cell populations. For the immune response, we model the evolution of effector (and effector-memory) cells in the lymphoid compartment (y_{el}) and in the periphery (y_{ep}), and the central memory cells (y_{cm}) in the lymphoid compartment. Finally, we model

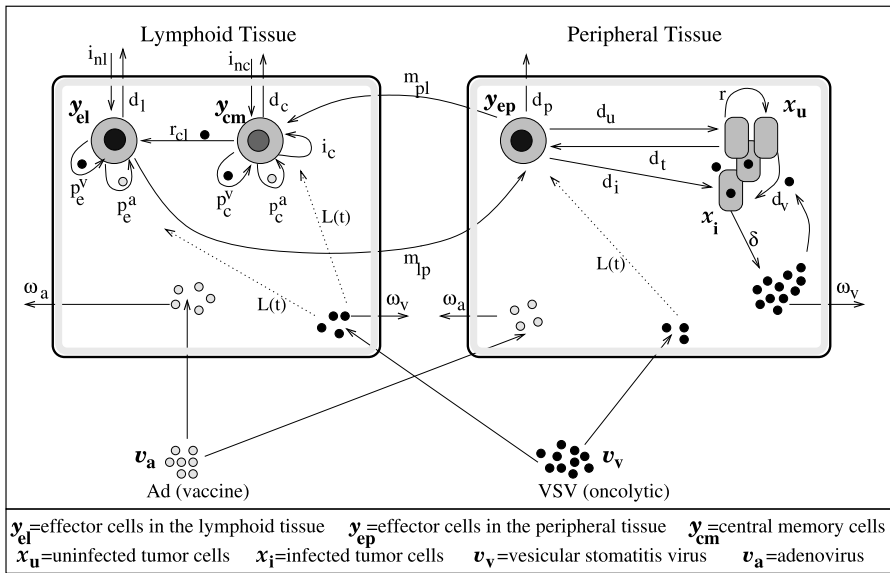


Fig. 1 Schematic representation of the interactions among immune cells, tumor cells, and virus particles. We focus on two compartments: the lymphoid tissue (where the immune cells are activated and undergo clonal expansion) and the peripheral tissue (where the tumor is localized)

the viral loads for the oncolytic virus (v_v) and the vaccine virus (v_a). These variables are summarized in Table 2 (Appendix B).

Before introducing the model, let us describe in detail the assumptions that we make about the cancer-immune-virus interactions. These assumptions are depicted schematically in Fig. 1.

- (i) *The dynamics of uninfected tumor cells (x_u).* We assume that tumor cells proliferate at an intrinsic rate r with logistic density dependence. These cells can become infected with the oncolytic virus at intrinsic rate d_v . Since viral replication and spread can be hindered by the architecture of the solid tumor (Breitbart et al. 2007), we consider a Michaelis–Menten term to describe these tumor-virus interactions: $\frac{x_u v_v}{h_u + x_u}$, where h_u is the half-saturation constant of tumor cells. Finally, the tumor cells are lysed at a rate d_u by the effector cells in the periphery. Again, tumor architecture can restrict the tumor-immune interactions (Blohm et al. 2006): we model this with a factor $\frac{x_u y_{ep}}{h_{ep} + y_{ep}}$, where h_{ep} is the half-saturation constant of immune cells.
- (ii) *The dynamics of infected tumor cells (x_i).* This cell population increases at a rate d_v , following the infection of tumor cells with the oncolytic virus. The infected cells are lysed by viruses at a rate δ , and by effector cells in the periphery at a rate d_i .
- (iii) *The dynamics of central memory cells (y_{cm}).* In the absence of any antigen, these cells can proliferate at a very slow rate i_c (Wherry et al. 2003; Sallusto et al. 2004). To maintain this pool of memory cells, proliferation is counterbalanced by a low death rate d_c (Marsden et al. 2006). In addition, there might be a

very low inflow (i_{nc}) of memory cells caused by the presence of tumor antigens (or some other antigens). These cells also proliferate following encounter with viral antigens (Marsden et al. 2006). We denote by p_c^a and p_c^v the proliferation rates in the presence of Ad and VSV antigens, respectively. Since memory cells compete for space with other cells, we use a logistic function to describe their proliferation: $y_{cm}(1 - k_c y_{cm})$. In addition, cell proliferation in response to viral antigens is described by

$$P(v_{a,v}) = \frac{v_{a,v}}{h_{a,v} + v_{a,v}}. \quad (1)$$

This sigmoidal function can account for the different observations regarding the level and duration of antigen stimulation necessary to induce clonal expansion (Kaech et al. 2002; Finn et al. 2009; Turner et al. 2007; de Boer et al. 2001). Parameters $h_{a,v}$ describe the amount of antigen (or virus particles) necessary to generate half-maximal stimulation. The full terms describing the proliferation of memory cells in response to Ad and VSV particles/antigens are: $p_c^{a,v} P(v_{a,v}) y_{cm}(1 - k_c y_{cm})$.

The secondary encounter with the tumor-associated antigen causes memory cells to proliferate quickly and then differentiate to effector cells (Sallusto et al. 2004). This differentiation process, which depends on the presence of viral antigen (Wherry et al. 2003), is described by $r_{cl} \frac{v_v y_{cm}}{h_v + v_v}$.

We assume that the population of memory cells can also increase through the survival and migration to the lymphoid tissue of effector and effector-memory cells following the contraction phase of the immune response (Wherry et al. 2003; Marsden et al. 2006). The migration process, which is assumed to be reduced in the presence of antigen (Kaech et al. 2002; Wherry et al. 2003), is described by $\frac{m_{pl} y_{ep}}{1 + g_v v_v}$. Here, m_{pl} is the very low migration rate, and $1/g_v$ is the concentration of VSV antigen at half maximum.

Finally, the early stages of VSV infection are characterized by a severe lymphopenia, which results in a reduction of $CD8^+$ T cell numbers for 2–4 days following the infection (Bahl et al. 2006; Schattner et al. 1983). This reduction, which affects mainly memory cells, can be described mathematically by $l_c L(t) y_{cm} v_v$, where

$$L(t) = e^{-q|t-t_0|}. \quad (2)$$

Here, $1/q$ is related to the duration of virus-induced lymphopenia, while l_c is the reduction rate of $CD8^+$ T cells.

- (iv) *The dynamics of effector (and effector-memory) cells in the lymphoid tissues* (y_{el}). First, there is a very low, constant influx (i_{nl}) of cells into the lymphoid tissue (caused, for example, by the presence of tumor antigens). Cell numbers can also increase following encounter with viral antigens: $p_e^{a,v} P(v_{a,v}) y_{el}(1 - k_e y_{el})$. Here, $p_e^{a,v}$ are the proliferation rates. The logistic term describes a self-limitation process with carrying capacity $1/k_e$. (Effector cells produce molecules such as IFN- γ and perforin, which limit their growth (Badovinac et al. 2000).)

The number of effector cells can also increase following the expansion and differentiation (at a rate r_{cl}) of memory cells into effector cells (Sallusto et al. 2004).

Finally, cell numbers are reduced as a result of cell death (at a rate d_l), migration to the peripheral tissue (at a rate m_{lp}), and virus-induced lymphopenia (at a rate l_1).

- (v) *The dynamics of effector (and effector-memory) cells in the periphery (y_{ep}).* The effector cells arrive in the peripheral tissue following migration (at a rate m_{lp}) from the lymphoid tissues. The decline in the number of effector cells is the result of cell death (at a rate d_p) or virus-induced lymphopenia (at a rate l_1). Finally, the effector cells in the periphery are inactivated (at a rate d_t) following interactions with the uninfected tumor cells.
- (vi) *The dynamics of the oncolytic vesicular stomatitis virus (v_v).* The virus is injected on day $t_0 > 0$ following a pulse-like treatment $c_v(t)$:

$$c_v(t) = \begin{cases} 10^7 \frac{\text{PFU}}{(\mu\text{L})(\text{day})}, & \text{if } t \in [t_0, t_0 + 1], \\ 0, & \text{otherwise,} \end{cases} \tag{3}$$

where PFU/ μl denotes ‘‘plaque forming units per μl of blood’’. When an infected tumor cell dies (at a rate δ), it releases b virus particles. Finally, the virus is eliminated by various cells (e.g., Kupffer cells) at a rate ω_v (Brunner et al. 1960).

- (vii) *The dynamics of the adenovirus vaccine (v_a).* The virus, which is injected into the tumor-bearing mice on day 0, is eliminated rapidly (at a rate ω_a) by various immune cells (Alemany et al. 2000).

Putting together all the above assumptions, leads to the following equations, which describe the interactions among tumor cells, immune cells, and viral particles:

$$\frac{dx_u(t)}{dt} = rx_u(1 - k(x_u + x_i)) - d_v \frac{x_u v_v}{h_u + x_u} - d_u \frac{x_u y_{ep}}{h_{ep} + y_{ep}}, \tag{4a}$$

$$\frac{dx_i(t)}{dt} = d_v \frac{x_u v_v}{h_u + x_u} - \delta x_i - d_i \frac{x_i y_{ep}}{h_{ep} + y_{ep}}, \tag{4b}$$

$$\begin{aligned} \frac{dy_{cm}(t)}{dt} &= i_{nc} + y_{cm}(i_c + p_c^a P(v_a) + p_c^v P(v_v))(1 - k_c y_{cm}) \\ &\quad + m_{pl} \frac{y_{ep}}{1 + g_v v_v} - r_{cl} \frac{v_v y_{cm}}{h_v + v_v} - d_c y_{cm} - l_c L(t) y_{cm} v_v, \end{aligned} \tag{4c}$$

$$\begin{aligned} \frac{dy_{el}(t)}{dt} &= i_{nl} + y_{el}(p_e^a P(v_a) + p_e^v P(v_v))(1 - k_e y_{el}) + r_{cl} \frac{v_v y_{cm}}{h_v + v_v} \\ &\quad - d_l y_{el} - m_{lp} y_{el} - l_1 L(t) y_{el} v_v, \end{aligned} \tag{4d}$$

$$\frac{dy_{ep}(t)}{dt} = m_{lp} y_{el} - d_p y_{ep} - d_t x_u y_{ep} - m_{pl} \frac{y_{ep}}{1 + g_v v_v} - l_1 L(t) y_{ep} v_v, \tag{4e}$$

$$\frac{dv_v(t)}{dt} = c_v(t) + \delta b x_i - \omega_v v_v, \quad (4f)$$

$$\frac{dv_a(t)}{dt} = -\omega_a v_a. \quad (4g)$$

Note that (4f) does not include a term of the form

$$-d_v \frac{x_u v_v}{(h_u + x_u)}, \quad (5)$$

which would model the removal of free virus particles. Once a virus enters a tumor cell, it cannot infect other cells, and thus it cannot be part of the free virus population. This assumption was incorporated into the mathematical models of Bajzer et al. (2008), Dingli et al. (2009), Biesecker et al. (2010) and references therein. However, many other models do not incorporate such a term (e.g., Friedman et al. 2006; Wu et al. 2004; Ferreira et al. 2005; Paiva et al. 2009). The question comes down to whether successful cell entry represents a significant loss term for free virus. We tested the sensitivity of our model to this assumption with numerical simulations. We found that while this term slightly changes one of the steady states, it does not have a significant impact on the overall dynamics of system (4). For this reason, we chose to leave it out and avoid complicating the model further.

In the following, we will investigate the effect of the linear and nonlinear tumor-immune-virus interactions on the local and global dynamics of this model.

3 Linear Analysis of Steady States

We begin investigating the behavior of system (4) by discussing first the steady state solutions. System (4) can evolve toward a tumor-free steady state, or toward various tumor-present steady states.

1. The tumor-free (TF) steady state is described by

$$(x_u, x_i, y_{cm}, y_{el}, y_{ep}, v_v, v_a) = (0, 0, y_{cm}^{*,0}, y_{el}^{*,0}, y_{ep}^{*,0}, 0, 0), \quad (6)$$

with

$$y_{el}^{*,0} = \frac{i_{nl}}{d_l + m_{lp}}, \quad (7a)$$

$$y_{ep}^{*,0} = \frac{m_{lp} y_{el}^{*,0}}{d_p + m_{pl}}, \quad (7b)$$

$$y_{cm}^{*,0} = \frac{i_c - d_c + \sqrt{(i_c - d_c)^2 + 4i_c k_c (i_{nc} + m_{pl} y_{ep}^{*,0})}}{2i_c k_c}. \quad (7c)$$

2. The first tumor-present steady state does not depend on the oncolytic virus:

$$(x_u, x_i, y_{cm}, y_{el}, y_{ep}, v_v, v_a) = (x_u^*, 0, y_{cm}^*, y_{el}^*, y_{ep}^*, 0, 0). \quad (8)$$

Here,

$$y_{el}^* = \frac{i_{nl}}{d_l + m_{lp}}, \quad (9a)$$

$$y_{ep}^* = \frac{m_{lp}y_{el}^*}{d_p + d_t x_u^* + m_{pl}}, \quad (9b)$$

$$y_{cm}^* = \frac{i_c - d_c + \sqrt{(i_c - d_c)^2 + 4i_c k_c (i_{nc} + m_{pl}y_{ep}^*)}}{2i_c k_c}, \quad (9c)$$

$$x_u^* = \frac{r - d_u \frac{y_{ep}^*}{h_{ep} + y_{ep}^*}}{rk}. \quad (9d)$$

This tumor-only (TO) steady state (i.e., tumor without virus) exists when

$$r > d_u \frac{y_{ep}^*}{h_{ep} + y_{ep}^*}. \quad (10)$$

Using (9b), we can rewrite this inequality as

$$\frac{m_{lp}y_{el}^*}{d_p + d_t x_u^*} < \frac{r h_{ep}}{d_u - r}. \quad (11)$$

We now observe that (11) (or (10)) is likely to be satisfied for large h_{ep} . (Parameter r is usually fixed, since it depends on how aggressive the tumor is.) Parameter h_{ep} is related to the number of tumor-infiltrated immune cells necessary for an optimal killing of tumor cells. Since this parameter could be changed experimentally (see the discussion in Sect. 5), in the next sections we will investigate its role on the dynamics of system (4).

Using (9b) and (9d), one can show that system (4) could have at most two TO steady states, $x_u^{*,1}$ and $x_u^{*,2}$. These states are given by (see also Fig. 5):

$$x_u^{*,1,2} = \frac{-B \pm \sqrt{B^2 - 4AC}}{2A}, \quad (12)$$

with

$$A = rkh_{ep}d_t, \quad (13a)$$

$$B = rkh_{ep}(d_p + m_{pl}) + rkm_{lp}y_{el}^* - rh_{ep}d_t, \quad (13b)$$

$$C = -rh_{ep}(d_p + m_{pl}) + (d_u - r)m_{lp}y_{el}^*. \quad (13c)$$

Note that when $B < 0$ and $C > 0$ (which could happen only for large d_t) there are two positive steady states, $x_u^{*,1,2}$. On the other hand, when $B < 0$ and $C < 0$, or $B > 0$ and $C < 0$, there is only one positive steady state, $x_u^{*,1}$. This could happen if either of h_{ep} or r is sufficiently large.

Corresponding to these $x_u^{*,1,2}$ states, there are two different states for the effector cells: $y_{ep}^{*,1,2}$. We will revisit these states in the next section.

3. The second tumor-present steady state depends on the oncolytic virus (v_v):

$$(x_u, x_i, y_{cm}, y_{el}, y_{ep}, v_v, v_a) = (x_u^{*,v}, x_i^{*,v}, y_{cm}^{*,v}, y_{el}^{*,v}, y_{ep}^{*,v}, v^*, 0). \tag{14}$$

We will denote this steady state by TV (“tumor with virus”). Because of the complexity of (4), it is impossible to obtain closed-form expressions for the states described by (14). (Finding the steady states would amount to finding the roots of a polynomial of degree higher than four.) However, using (4b) and (4f), one can show that the TV state exists only when

$$d_v \frac{x_u^{*,v}}{h_u + x_u^{*,v}} - \frac{\omega_v}{\delta b} \left(\delta + d_i \frac{y_{ep}^{*,v}}{h_{ep} + y_{ep}^{*,v}} \right) = 0. \tag{15}$$

This equation depends on the parameters describing the dynamics of the oncolytic virus. To understand it, let us introduce the effective reproduction number, R_e^v , which is a measure of the infection of tumor cells with the oncolytic virus (see also Nowak and May 2000 for a discussion on how to calculate R_e^v):

$$R_e^v = \frac{d_v \delta b \frac{x_u^{*,v}}{h_u + x_u^{*,v}}}{\omega_v \left(\delta + d_i \frac{y_{ep}^{*,v}}{h_{ep} + y_{ep}^{*,v}} \right)}. \tag{16}$$

Now, it becomes clear that (15) is equivalent to $R_e^v = 1$. Note that the state variables in (16) are actually described in terms of the model parameters. However, since the exact formulas for these variables are very complex, throughout this article we will work directly with $x_u^{*,v}$ and $y_{ep}^{*,v}$.

The expression for R_e^v is slightly different than the effective reproduction number R_e^o associated with the TO state:

$$R_e^o = \frac{d_v \delta b \frac{x_u^{*,1,2}}{h_u + x_u^{*,1,2}}}{\omega_v \left(\delta + d_i \frac{y_{ep}^{*,1,2}}{h_{ep} + y_{ep}^{*,1,2}} \right)}. \tag{17}$$

Here, the tumor ($x_u^{*,1,2}$) and immune ($y_{ep}^{*,1,2}$) states do not depend on the virus (v^*). Since the virus contributes to the elimination of tumor cells $x_u^{*,v}$, we expect that

$$x_u^{*,v} < x_u^{*,1}. \tag{18}$$

It is possible in principle that some of $x_u^{*,v}$ are greater than $x_u^{*,2}$. However, throughout most of this article (with the exception of Sect. 4.1), we focus on the parameter regime where $x_u^{*,2}$ does not exist.

Figure 2 depicts graphically the surfaces describing the two effective reproduction numbers, R_e^o and R_e^v . We choose to focus on two parameters, d_u and ω_v , since they can be manipulated experimentally (see also the discussion in Sect. 5). Note that for $x_u^{*,v}$ close to $x_u^{*,1}$, the TV state exists only when $\omega_v < \omega^*$ (Fig. 2(b)). This corresponds to $R_e^o > 1$ (Fig. 2(a)). The parameter values used to calculate these

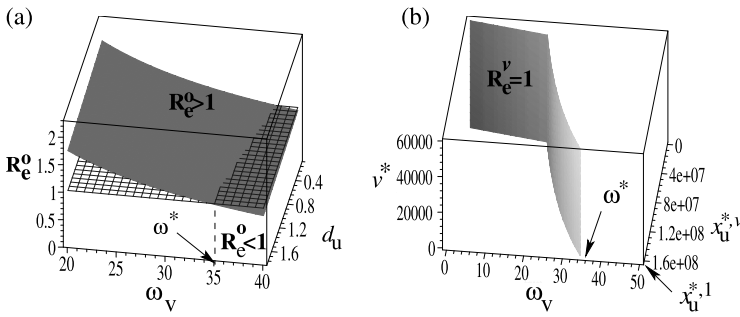


Fig. 2 (a) Graphical depiction of R_e^o as two parameters are varied at the same time: the rate at which the immune cells eliminate the tumor cells (d_u), and the rate at which the oncolytic virus is eliminated (ω_v). For $d_u \in [0.1, 1.8]$, R_e^o crosses the threshold $R_e^o = 1$ at a value $\omega_v = \omega_v^* \in [34.51, 37]$. In particular, when $d_u = 1.8$, $\omega_v^* = 34.51$. (b) Graphical depiction of the surface generated by $R_e^v = 1$, for a wide range of tumor sizes ($x_u^{*,v}$) and viral loads (v^*) (see (16)). Note that, for $x_u^{*,v} \leq x_u^{*,1}$ (where $x_u^{*,1}$ denotes the only positive tumor size for the TO steady state), $R_e^v = 1$ only when $\omega_v \leq \omega_v^*$. Here, $d_u = 1.8$, $l_c = 9.45 \times 10^{-6}$, $l_1 = 4.5 \times 10^{-7}$, $h_v = 10^4$, $h_a = 10^{-2}$, $i_{nc} = 0$. The rest of parameter values are given in Table 1 (Appendix B)

two surfaces are given in the caption of Fig. 2 and in Table 1 (Appendix B). We will revisit these TV states in the next section.

Remarks When $i_{nl} = i_{nc} = m_{pl} = 0$, there is no long-term immune response: $y_{el}^* = y_{cm}^* = y_{cm}^* = 0$. If, in addition $d_c = i_c = 0$, then in the absence of the oncolytic virus ($v^* = 0$) memory cells can approach an infinite number of states y_{cm}^* . (There is an entire line of values for y_{cm}^* .)

3.1 Stability of Steady States

In the following, we will present the analytical conditions necessary for the stability of the virus-free steady states. The stability of the TV state will be investigated numerically.

To begin, the stability of the tumor-free (TF) steady state (6) is given by the sign of the first eigenvalue (λ_1) of the Jacobian matrix associated with system (4). (All other eigenvalues are always negative.)

$$\lambda_1 = r - \frac{d_u y_{ep}^{*,0}}{h_{ep} + y_{ep}^{*,0}}. \tag{19}$$

Lemma 1 *The TF steady state (6) is*

(a) *Stable when*

$$r < \frac{d_u y_{ep}^{*,0}}{h_{ep} + y_{ep}^{*,0}}. \tag{20}$$

In this case, the steady state is a stable node.

(b) *Unstable when*

$$r > \frac{d_u y_{ep}^{*,0}}{h_{ep} + y_{ep}^{*,0}}. \quad (21)$$

In this case, the steady state is a saddle point.

Note that the TF and TO states are defined by slightly different effector cell numbers (see (7b) and (9b)). This allows for the possibility that (20) and (10) are both satisfied when d_t is large enough. In this case, it could be possible to have a bi-stability phenomenon between the TF and the TO states. We will investigate this possibility further in Sect. 4.1.

When the TO state (8) exists, its stability is determined by the value of the effective reproduction number R_e^o , as well as the immune response.

Lemma 2 *The TO steady state (8) is*

(a) *Stable when*

$$R_e^o < 1 \quad \text{and} \quad \left(\frac{y_{ep}^{*,1,2}}{h_{ep} + y_{ep}^{*,1,2}} \right)^2 < \frac{rkm_{lp}i_{nl}}{(d_l + m_{lp})d_u h_{ep} d_t}. \quad (22)$$

In this case, the steady state is a stable node.

(b) *Unstable when*

$$R_e^o > 1 \quad \text{or} \quad \left(\frac{y_{ep}^{*,1,2}}{h_{ep} + y_{ep}^{*,1,2}} \right)^2 > \frac{rkm_{lp}i_{nl}}{(d_l + m_{lp})d_u h_{ep} d_t}. \quad (23)$$

In this case, the steady state is a saddle point.

A sketch of the proof is given in [Appendix A](#).

An analytical investigation of the stability of TV steady states is almost impossible. However, one can calculate numerically both the TV states and the eigenvalues of the Jacobian matrix corresponding to these states. Figure 3 shows the eigenvalues of a particular TV state when the parameter ω_v is decreased. (We choose to focus on parameter ω_v since it appears in R_e^o and R_e^v , and it can be manipulated experimentally.) We observe that for large ω_v ($\omega_v > 30$), the TV state is always stable (a stable focus or a stable node). For smaller ω_v ($\omega_v < 30$), the TV state is an unstable focus. The parameter values used to calculate these eigenvalues are given in the caption of Fig. 3 and in Table 1.

Note that the TV state investigated in Fig. 3 is not unique. Usually, when $\omega_v < 34$ there are at least two other TV states that are unstable foci and/or saddle points (not shown here).

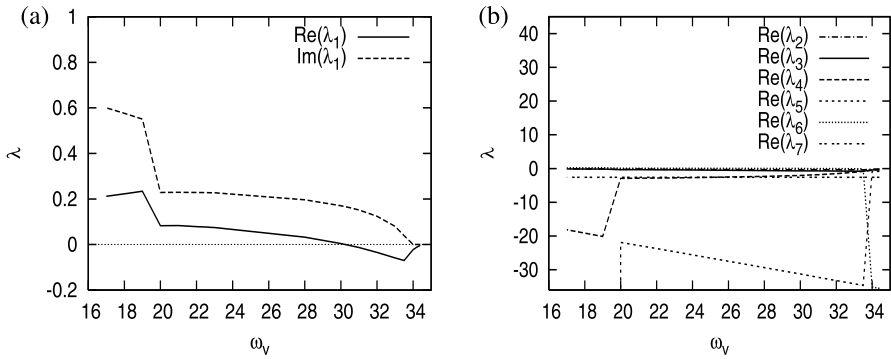


Fig. 3 Stability of a particular TV steady state, as given by the sign of the eigenvalues $\lambda_j, j = 1, \dots, 7$, of the Jacobian matrix. To compute the eigenvalues, we first calculated numerically the TV states corresponding to different values of $\omega_v \in (16.5, 34)$. (These states were calculated in Maple using `solve` command to find the solutions of a 7×7 system of algebraic equations.) We then used these TV states to calculate the Jacobian matrix associated with system (4). (a) The eigenvalue λ_1 is responsible for the change in stability. In particular, for $\omega_v > 30$, $\text{Re}(\lambda_1) < 0$ and the TV state is a stable focus ($\omega_v \in (30, 34)$) or a stable node ($\omega_v > 34$). For $\omega_v < 30$, $\text{Re}(\lambda_1) > 0$ and $\text{Im}(\lambda_1) > 0$, and the TV state is an unstable focus. (b) The eigenvalues $\lambda_j, j = 2, \dots, 7$. Note that for $\omega_v < 30$, the eigenvalue λ_6 is the complex conjugate of the eigenvalue λ_1 , and hence its real part is positive. All other eigenvalues are always negative. For these simulations, we used $d_u = 1.8, I_c = 9.45 \times 10^{-6}, I_1 = 4.5 \times 10^{-7}, h_v = 10^4, h_a = 10^{-2}, i_{nc} = 0$. The rest of parameter values are given in Table 1 (Appendix B)

4 Numerical Results

We begin discussing the dynamics of model (4) by investigating the short-time behavior of this system. The initial conditions for the numerical simulations follow the experimental protocol of Bridle et al. (2009). We assume that “day 0” is the day when 10^6 PFU/ μl of Adenovirus (Ad) are injected: $v_a(0) = 10^6$. The rest of initial conditions are: $x_u(0) = 10^6, x_i(0) = 0, y_{cm}(0) = 0.01, y_{el}(0) = 1.5, y_{ep}(0) = 1.5$, and $v_v(0) = 0$. The parameter values used for these simulations are given in Table 1 (Appendix B).

Figure 4 shows the dynamics of system (4) following a standard immunization treatment (with Ad alone) or a sequential treatment (with Ad and VSV). (In the absence of any treatment, the tumor grows logistically and the immune response is almost non-existent (not shown here).) The immune response following Ad injection (Fig. 4(b)) leads to a slow decrease in tumor size, followed by a rapid tumor regrowth (Fig. 4(a)). The tumor reaches maximum size between 30–40 days. This is consistent with the experimental results in Bridle et al. (2010). When the oncolytic virus is introduced (Figs. 4(c) and (d)), the immune response increases significantly. This leads to a much higher reduction in tumor size, and a longer time until the tumor grows back. The results are consistent with murine experiments showing an increased secondary immune response following the injection of the oncolytic virus (VSV) (see Figs. 2 and S1 in Bridle et al. 2010). We note here an increased level of memory cells following the administration of the second virus.

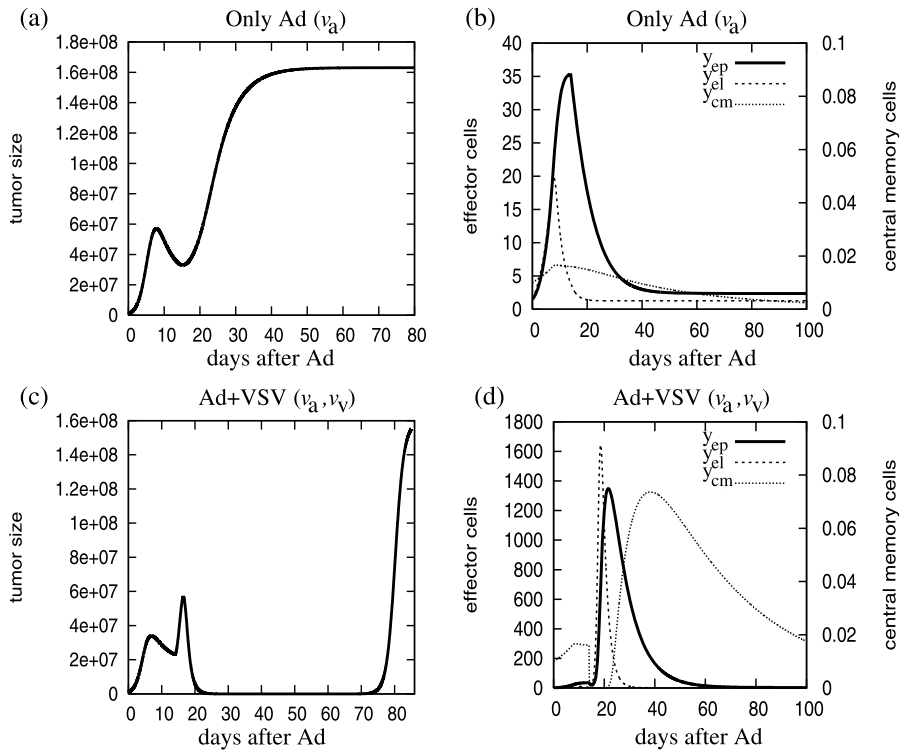


Fig. 4 (a) Tumor size in the absence of the oncolytic virus (only the Ad vaccine is given). (b) The magnitude of the memory and effector immune responses following the boost with the vaccine virus. (c) Tumor size following the administration of the dual treatment: vaccine virus on day 0, and oncolytic virus on day 14. (d) The magnitude of the memory and effector immune responses following the dual treatment. The parameter values for these simulations are: $\omega_v = 40$, $h_v = 10^4$, $h_a = 10^{-2}$, $i_{nc} = 0$. The rest of the parameter values are given in Table 1 (in Appendix B)

This high level is important since it could theoretically control subsequent tumor relapses.

In Fig. 4(d), we also observe an immediate decrease in the immune response caused by the introduction of the VSV on day 14 (i.e., virus-induced lymphopenia). Detailed numerical simulations (not shown here) suggest that by increasing the duration of the immune suppression, one can obtain a higher immune response later. This is the indirect result of larger tumors and better viral replication, which leads to better proliferation of immune cells.

For the parameter values used in these simulations, the tumor always grows back. Here, the only non-negative TO state, $x_u^{*,1}$, is always stable. The TF steady state $x_u^{*,0}$ is always unstable. The permanent elimination of tumor cells, which is observed in certain experiments (Bridle et al. 2010), could be explained in system (4) by higher d_u rates (see also the discussion in Sect. 3.1).

We also tested numerically what happens when we consider injecting only one virus, either the oncolytic virus (VSV) or the vaccine virus (Ad). (For both cases, we took $p_e^a = p_e^v = 0.6$ and $p_c^a = p_c^v = 0.09$ to be the immune proliferation rates

in the absence of immunological memory. The rest of the parameters were chosen as in Fig. 4). The results suggested that even if we increase the dose of each virus by ten fold, the single treatment protocols are not as effective against the tumor as the sequential treatment discussed in Fig. 4(c) (when both viruses are given). More precisely, increasing the Ad dose from 10^6 PFU/ μ l to 10^7 PFU/ μ l delays tumor regrowth by 2–3 days (compared to the dynamics shown in Fig. 4(a)). Increasing the VSV dose from 10^7 PFU/ μ l to 10^8 PFU/ μ l cannot stop tumor growth: the tumor will reach its carrying capacity before it can be shrunk by the immune response. We infer that the sequential treatment is better than just giving a higher dose of one of the two viruses.

So far, we have discussed the patterns exhibited by system (4) from the perspective of conditions that determine the local stability of the steady states. In the following, we will focus on the global behavior of system (4), and discuss two mechanisms that could alter the final steady state patterns. These two mechanisms are *multi-stability* and *multi-instability*.

4.1 Multi-Stability for the Tumor-Immune-Virus Dynamics

The *multi-stability* phenomenon is caused by the presence of multiple steady states that are stable at the same time. (If there are only two stable steady states, we call it a *bi-stability* phenomenon.) In cancer immunology, the existence of such a phenomenon can provide information on the conditions that could cause a sudden transition from a tumor-present to a tumor-free steady state (and vice versa).

As seen in Sect. 3, for some parameters it is possible to have three steady states: one tumor-free (TF) and two tumor-present (TO) states. Figure 5 shows the dynamics of system (4) in a region of the parameter space characterized by relatively high rates for the tumor-induced inactivation of effector cells ($d_t = 2.98 \times 10^{-9}$) and very high tumor killing rates ($d_u = 15.8$). To investigate the transition between the different steady states, we focus on the parameter h_{ep} . This parameter is related to the concentration of effector immune cells necessary to be present in the tumor to ensure half the maximum killing rate (see also the discussion in Sect. 5). For intermediate values of h_{ep} ($h_{ep} \in (35, 50)$), we observe a bi-stable behavior between the TF steady state and one of the TO steady states (Fig. 5(a)). (Here, there is no TV state since $R_c^o < 1$.) This behavior can explain the abrupt changes in tumor size as one parameter is gradually increased. In particular, we note that tumors with sizes above the dashed curve (which describes the unstable state $x_u^{*,2}$) will continue growing until they reach the stable state $x_u^{*,1}$. This has implications on the treatment protocol. In particular, treatment does not have to be administered until the complete elimination of the tumor. It is enough to treat the tumor until its size decreases below the dashed curve. Then the solution of system (4) will be attracted by the stable tumor-free steady state.

This bi-stable behavior is accompanied by a hysteresis phenomenon. As h_{ep} is increased, the tumor-free steady state loses stability and the system evolves toward the higher tumor-present steady state ($x_u^{*,1}$). If h_{ep} is now decreased below $h_{ep} = 50$,

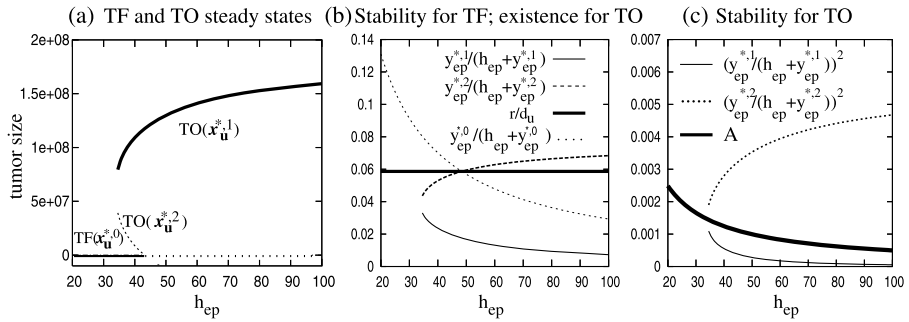


Fig. 5 Graphical description of the existence and stability conditions for the TF (6) and the TO (8) steady states. (a) For small h_{ep} , there is only one steady state: the TF state which is stable (*the continuous line*). As h_{ep} increases slowly, there is a saddle-node bifurcation that gives rise to another two steady states: the TO states. The first state is stable (*the continuous curve*), while the second one is unstable (*the dotted curve*). As h_{ep} increases further, the second state disappears through a subcritical bifurcation at $h_{ep} \approx 50$. (b) Graphical description of inequalities (20)–(21) and (10), which determine the stability of the TF steady state (corresponding to $y_{ep}^{*,0}$) and the existence of the TO steady states (corresponding to $y_{ep}^{*,1}$ and $y_{ep}^{*,2}$). (c) Graphical description of the second part of inequalities (23) and (22), which give the stability of the two TO states (13). The parameter A is given by $A = \frac{rkm_{ip}i_{nl}}{d_u d_1 h_{ep} (d_1 + m_{ip})}$. The first steady state (corresponding to $y_{ep}^{*,1}$) satisfies inequality (23), while the second state (corresponding to $y_{ep}^{*,2}$) satisfies inequality (22). Here, $d_u = 15.8$, $d_t = 2.89 \times 10^{-9}$, $l_c = 9.45 \times 10^{-6}$, $l_1 = 1.845 \times 10^{-5}$, $h_v = 10^4$, $h_a = 10^{-2}$ and $i_{nc} = 0$. The rest of the parameter values are specified in Table 1 (Appendix B)

the system does not return immediately to its initial tumor-free steady state. It will return to this state later, when $h_{ep} \approx 35$.

Figure 5(b) depicts graphically the conditions that ensure the existence of TO steady states and the stability of TF steady state ((10) and (20)–(21)). As h_{ep} increases past the value $h_{ep} = 50$, the TF state loses its stability (the dotted curve goes below the line r/d_u). At the same point, one of the TO states disappears (the dashed curve is now above the horizontal line r/d_u). Figure 5(c) depicts graphically the second part of inequalities (22)–(23), which describe the stability of the TO steady states. We note here that the two steady states have opposite stabilities (the continuous and the dotted curves are above and below the thick continuous curve described by $A = \frac{rkm_{ip}i_{nl}}{d_u d_1 h_{ep} (d_1 + m_{ip})}$).

We note that, for the parameter values investigated in Fig. 5, it is not possible to have both TO steady states stable. However, since the parameter space is very large, we cannot exclude the possibility that for some specific parameter values all virus-free states could be stable at the same time.

To conclude, the existence of a bi-stable or, more generally, a multi-stable regime for the tumor-free and tumor-present steady states could explain the transitions between these states during the evolution of cancer. In particular, environmental stochasticity could push the system from one state to the other. Thus, relatively large tumors could disappear even in the absence of external treatment, and tumors that were thought to be in remission could relapse again.

4.2 Multi-Instability for the Tumor-Immune-Virus Dynamics

In this section, we discuss a more complex phenomenon exhibited by model (4), namely multi-instability. As we will show next, this phenomenon, too, could cause a transition from a tumor-present to a tumor-free steady state.

Inequality (23) suggests that condition $R_c^o > 1$ is sufficient to cause the TO steady states to become unstable. Note that R_c^o depends mainly on the parameters governing the dynamics of the oncolytic virus (v_v). Hence, the stability/instability of TF steady state (which depends only on the immune response) can be decoupled from the instability of TO steady states. Moreover, Figs. 2(b) and 3(a) suggest that when $R_c^o > 1$ the TV steady states exist and can also be unstable. This leads to the possibility of having a parameter regime where all equilibria (i.e., TF, TO, and TV) are unstable. This is called a *multi-instability* phenomenon. (Note that, if there are only two states and they are both unstable, this is usually called a *bi-instability* phenomenon.)

Figure 6 describes the long-term dynamics of system (4), as the parameter ω_v is decreased past the threshold value $\omega_v^* = 34.51$ (obtained for $R_c^o = 1$). (All other parameters are fixed and their values are described in the caption of Fig. 6 and in Table 1.) For large ω_v (and $R_c^o < 1$), the system evolves toward the TO steady state $x_u^{*,1}$ (Fig. 6(b)). The figure in the inset shows the absence of the oncolytic virus. Note that for the parameter values used in these simulations, the state $x_u^{*,2}$ is negative. Figure 6(c) shows that as we decrease ω_v ($\omega_v \in (30, 34.51)$), the dynamics of the system approaches the TV state. This state, which is characterized by the presence of the virus and a slightly smaller tumor size, is stable for $\omega_v > 30$ (see also Fig. 3). As ω_v is decreased further ($\omega_v \in (22.7, 30)$), the system approaches a limit cycle, where both the tumor and the virus are present (Fig. 6(d)). The amplitude of these oscillations increases as ω_v decreases. We will refer to these oscillations as “spike-like” oscillations. Here, all steady states are unstable (see also Fig. 3 for the stability of TV state). If we decrease ω_v below the critical value 22.7, the oscillations become more complex, involving all three steady states: TF, TO, and TV (Fig. 6(e)). Actually, the transition from the TO state to the TF state happens as the solution passes near the TV state. In particular, in Fig. 6(e), we note a lower tumor size toward the end of the tumor peaks. This corresponds to a peak in the virus load (i.e., a TV state). We will refer to these oscillations as “plateau-like” oscillations. Here, the TF and TO equilibria are unstable saddle points, while the TV equilibria are either saddle points or unstable foci (see also Fig. 3). Finally, for very small values of ω_v , system (4) evolves toward a tumor-free state (Fig. 6(f)). Note that in this case, the oncolytic virus can be detected in the system for 10–11 days after it was introduced (compared to only 4–5 days when $\omega_v > 30$). Here, we consider the detection threshold to be $v_v \geq 1000$ particles.

Note that the dynamics shown in Fig. 6 are not sensitive to the initial conditions. Small changes in the initial tumor size or in the initial immune response will influence only the short-term dynamics of system (4) (described in Fig. 4). They will not have any effect on the long-term dynamics of this model.

Figure 7 shows a phase-plane representation of the patterns described in Figs. 6(d) and (e). Note that the period of oscillations increases as ω_v decreases. Close to the threshold value $\omega_v = \omega_v^{**} = 16.3$, the period becomes very large. As ω_v crosses this

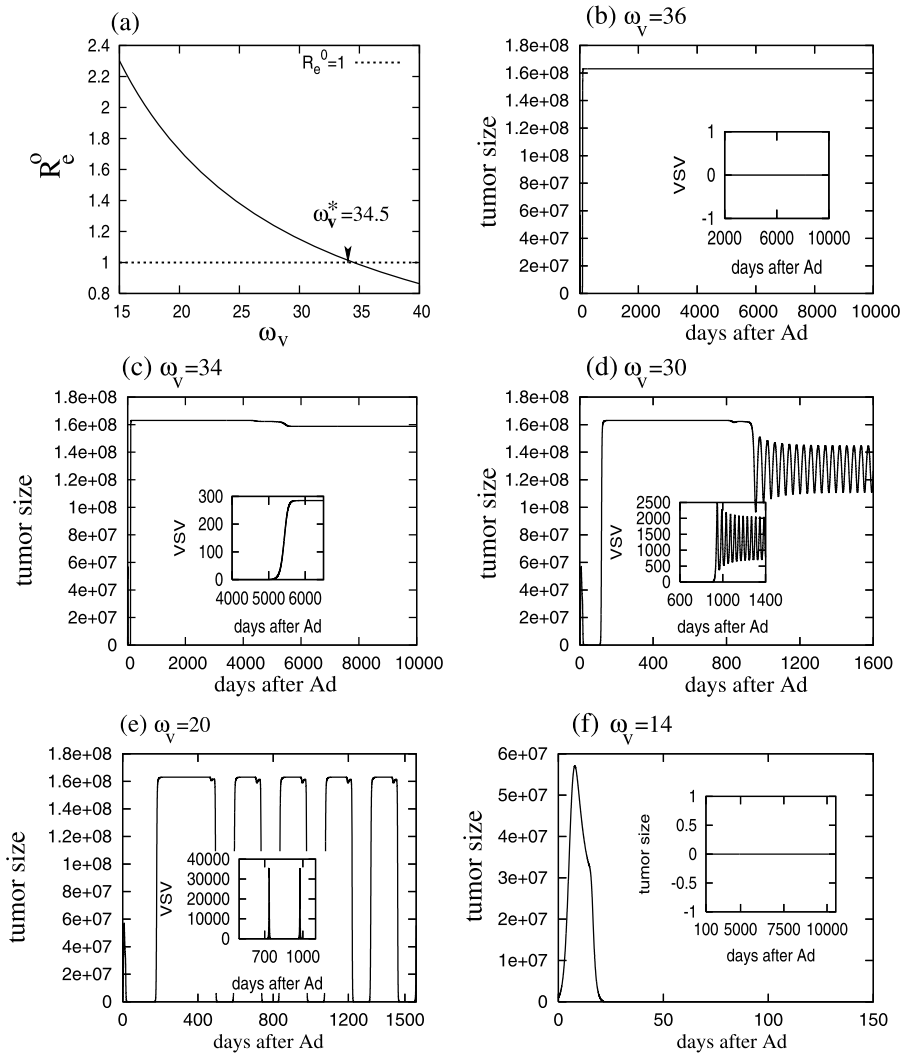


Fig. 6 The effect of decreasing ω_v on the long-term behavior of system (4). (a) Graphical depiction of R_e^0 as the rate at which the oncolytic virus is eliminated (ω_v) decreases. R_e^0 crosses the threshold $R_e^0 = 1$ when $\omega_v^* = 34.51$ (and $d_u = 1.8$). (b) The TO steady state (see (8)). The inset shows the absence of the oncolytic virus (VSV). (c) The TV steady state (see (14)). The inset shows the presence of the virus. (d) Oscillatory behavior for the TV state. (e) Oscillatory behavior that involves all three steady states. The solution spends a significant amount of time near the TF state or the TO state. To get from the TO to the TF state, the solutions first passes near the TV state (see the VSV values in the inset figure). (f) The TF steady state. For these simulations, we used $d_u = 1.8$, $l_c = 9.45 \times 10^{-6}$, $l_l = 4.5 \times 10^{-7}$, $h_v = 10^4$, $h_a = 10^{-2}$, $i_{nc} = 0$. The rest of parameter values are given in Table 1 (in Appendix B)

threshold, the dynamics changes drastically, and the system now evolves toward a tumor-free steady state (see also Fig. 6(f)). This suggests that at $\omega_v^{**} = 16.3$ there is a homoclinic bifurcation, which is characterized by a period of oscillations that becomes very large as $\omega_v \rightarrow \omega_v^{**}$. This “dangerous bifurcation” could explain the

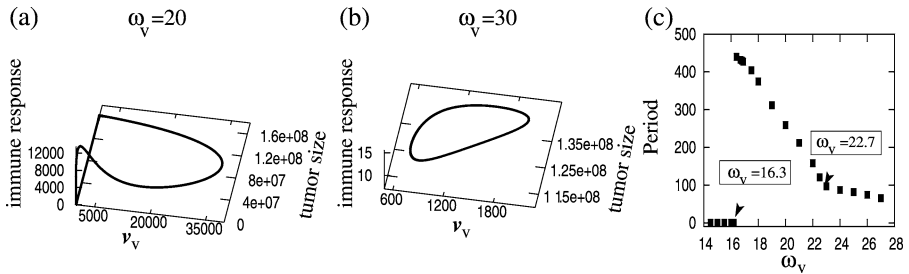


Fig. 7 Phase-plane dynamics for system (4), corresponding to the oscillatory patterns shown in Fig. 6. Here, we graph only the long-term behavior of this system ($t > 1500$ days). The immune response-axis shows the total number of immune cells: $y_{cm} + y_{el} + y_{ep}$. **(a)** For $\omega_v = 20$, the system evolves toward a homoclinic orbit. This corresponds to the plateau-like oscillations shown in Fig. 6(e). **(b)** For $\omega_v = 30$, the system evolves toward a limit cycle. This corresponds to the spike-like oscillations shown in Fig. 6(e). **(c)** The period of oscillations as a function of the parameter ω_v . (We calculated this period numerically, by computing the distance between two successive maximum points in the number of uninfected tumor cells. For $\omega_v > 22.7$, the oscillations describe only the TV state (since $v_v > 0$), while for $\omega_v < 22.7$ the oscillations describe the periodic transitions TO–TV–TF–TO.) A homoclinic bifurcation occurs at $\omega_v = 16.3$. Note that at $\omega_v = 22.7$, the decrease in the period slows down. This corresponds to a transition from plateau-like to spike-like oscillations. Here, $d_u = 1.8$, $l_c = 9.45 \times 10^{-6}$, $h_1 = 4.5 \times 10^{-7}$, $h_v = 10^4$, $h_a = 10^{-2}$, $i_{nc} = 0$. The rest of parameter values are given in Table 1 (Appendix B)

sudden disappearance of the periodic attractor and the jump to a distant unrelated attractor, where the tumor is eliminated permanently (Thompson et al. 1994). This new attractor contains the stable manifold of the tumor-free steady state (which is a saddle point).

Note that even if the virus dynamics (and in particular ω_v) can push system (4) toward a tumor-free state (as in Fig. 7(f)), the immune response is crucial. We tested the importance of the immune cells for the outcome of the treatment by removing the anti-tumor immune response ($d_u = 0$) while keeping, however, the anti-tumor viral response ($d_v \neq 0$). This is equivalent to injecting an oncolytic virus which does not carry tumor antigens. Figure 8 shows the outcome of this experiment. First, we observe that the tumor reaches its maximum size before is eventually eliminated (Fig. 8(a)). This is the result of having an immune response which cannot “see” the tumor to control it (due to a lack of tumor antigens). The decrease in tumor size is associated with a very large increase in viral load (Fig. 8(b)). We conclude from here that even if the virus can eventually kill the tumor by pushing the system toward the TF state, the existence of an anti-tumor immune response is necessary to prevent the tumor from growing too fast toward its maximum size. These results are consistent with the experimental data in Bridle et al. (2010), which shows that the lack of tumor antigens leads to a very poor survival.

Finally, we note that the oscillatory behavior shown in Figs. 6(d), (e) and 7(a), (b) is not biologically realistic (at least not for solid tumors). One can argue that this is just a mathematical artifact not observed during the periods of tumor growth. In fact, these oscillatory patterns are observed only after the tumor has reached its carrying capacity. Nevertheless, these results suggest that by increasing the persistence of the oncolytic virus (i.e., from virus being detected for 4–5 days to being detected for

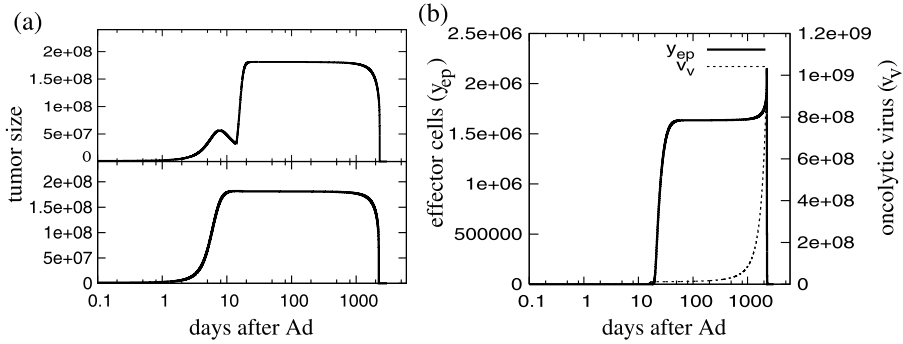


Fig. 8 The dynamics of system (4), when we alter the anti-tumor immune response. (a) The upper panel shows the tumor growth pattern when $d_u = 1.8$ for $t < t_0 = 14$, and $d_u = 0$ for $t \geq t_0$. This is equivalent to adding the tumor antigen to the vaccine virus (Ad), but not to the oncolytic virus (VSV). In this case the immune cells can “see” the tumor cells after the Ad, but not after the VSV. The lower panel shows the tumor growth pattern when $d_u = 0$ for all $t \geq 0$. This is equivalent to removing the tumor antigen from both viruses. In this case, the immune cells never “see” the tumor cells (they are virus-specific and not tumor-specific cells). (b) The effector immune response (y_{ep}) and the oncolytic virus load (v_v) corresponding to the tumor-growth patterns shown in panel (a). Note that the immune response reaches its maximum soon after day 14, following the introduction of the oncolytic virus. The decline in the immune response coincides with the elimination of the tumor and the oncolytic virus. Here, the parameters are: $\omega_v = 13.56$, $l_c = 9.45 \times 10^{-6}$, $l_1 = 4.5 \times 10^{-7}$, $h_v = h_a = 10^4$, $i_{nc} = 0$. The rest of parameter values are given in Table 1 (Appendix B)

10–11 days), one can push the system into a regime characterized by the permanent elimination of tumor cells.

5 Discussion and Biological Implications

In this article, we derived and investigated a non-spatial mathematical model that described the interactions among cancer cells, immune cells, and therapeutic viruses. The model followed a novel experimental protocol proposed by Bridle et al. (2010), which involved the sequential administration of two different viruses with the purpose of increasing the immune response. Despite the improved survival rates, the majority of mice in these experiments suffered tumor relapse (Bridle et al. 2010).

First, we showed that the mathematical model can exhibit exactly the same dynamics as the experimental observations. Numerical simulations revealed a secondary immune response much higher than the primary immune response. In addition, the results suggested that this response could be made even higher if we increase the immune suppression following the virus-induced lymphopenia.

Using this mathematical model, we then investigated the conditions that could ensure permanent tumor elimination. In particular, we focused on two complex phenomena, namely multi-stability and multi-instability. Both phenomena have the potential to induce sudden changes in the dynamics of a system.

The multi-stability phenomenon is characterized by the existence of multiple steady states that are simultaneously stable. The mathematical model derived in this

article exhibited a bi-stability phenomenon between a tumor-free and a tumor-present steady state. (Throughout this paper we referred, however, to the more general multi-stability phenomenon, since in a different parameter regime it might be possible to observe multiple stable steady states (i.e., the TO and TV states).) The bi-stable behavior was the result of the mutually inhibitory feedback between the tumor and the persistent immune response (Angeli et al. 2004). The indefinite persistence of effector cells—which required the assumption of indefinite persistence of tumor or viral antigens—was a necessary condition for the stability of the tumor-free steady state.

In addition to this bi-stability (or multi-stability) phenomenon (which has been previously described in models of tumor-immune interactions (Kirschner and Panetta 1998; Fiasconaro et al. 2008)), we also discussed the opposite phenomenon: the multi-instability phenomenon. This phenomenon was previously investigated in epidemiological models (Billings and Schwartz 2002; Choisy et al. 2006), but has not received much attention in models for tumor-immune-virus interactions. In our model, this phenomenon was associated with the long-time persistence of the oncolytic virus. (By “long-time persistence”, we mean that the virus can be detected in the system for 10–11 days, compared to its usual detection period of 4–5 days.) We showed that multi-instability, which was the result of all states being unstable at the same time, could push the dynamics of the system toward a tumor-free state. This was the result of a homoclinic bifurcation that triggered the sudden disappearance of the tumor-present attractor and the jump to a distant tumor-free attractor. The evolution of the system toward this tumor-free state could not have been predicted by the local analysis of the model.

We also tested whether the elimination of the tumor—which was caused by viral persistence—depended on the immune response. The results showed that suppressing the anti-tumor immune response while keeping intact the anti-viral immune response, could not stop tumor growth. Hence, an improvement in the treatment can occur only when both the anti-tumor immunity and the oncolytic activity are present.

The multi-instability phenomenon was observed only when the effective reproduction number was greater than one ($R_e^o > 1$). However, we cannot exclude the possibility of having a different bi-instability phenomenon when $R_e^o < 1$. This bi-instability could occur if the immune response causes both the TF and the TO states to become unstable (see inequalities (21) and (23)). However, we were unable to find parameter values that would ensure the instability of both these states.

Biological Implications First, we note that the simulation results for the dynamics of the tumor and immune cells are consistent with the experimental observations. For example, it was shown experimentally that the presence of CD8⁺ T cells is necessary to control the growth of the tumors during treatment with the vesicular stomatitis virus (VSV) (Diaz et al. 2007; Bridle et al. 2010). Bridle et al. (2010) showed that viral treatment has a poor outcome if the two viruses are administered alone (and not in combination), or if the viruses do not carry tumor antigens. In particular, mice survived on average for 30 days following treatment with Ad-hDCT (i.e., Ad carrying the tumor antigen hDCT), or for 20 days following treatment with VSV-hDCT (i.e., VSV carrying the tumor antigen hDCT). However, the combination of

Ad-hDCT and VSV-hDCT lead to an average survival of 50 days or more. Moreover, removing the tumor antigen from either virus decreased mouse survival. The mathematical model introduced in the present paper showed similar dynamics (see Figs. 4 and 8).

To investigate the bi-stability and multi-instability phenomena, we focused on three parameters: the rate at which the immune cells kill the tumor (d_u), the half-saturation constant for the effector cells that support half the maximum killing rate (h_{ep}), and the rate at which the oncolytic virus particles are eliminated from the system (ω_v). All these parameters can be changed during the experiments. For example, the first parameter, which is associated with the functionality of immune cells (i.e., their capacity to produce tumor-suppressing cytokines such as IFN- γ), could be changed by blocking the receptor programmed death-1 (PD-1) expressed on T cells (Curran et al. 2010). The second parameter, which is associated with the number of immune cells necessary for an optimal tumor cell lysis, could be experimentally modified by using antibody agonists against co-stimulatory molecules such as 4-1BB (Munks et al. 2004; Choi et al. 2007), or by blocking the PD-1 receptor (Curran et al. 2010). Finally, ω_v could be changed by blocking viral clearance by the reticulo-endothelial cells in the liver (Brunner et al. 1960).

We note that the model could have been simplified by investigating the ratio d_u/h_{ep} , which represents the slope of the anti-tumor immune response. However, experiments have shown that some treatments affect mainly the functionality of tumor cells (d_u), while others affect mainly the recruitment of immune cells inside the tumor (h_{ep}). By investigating separately the role of d_u and h_{ep} on the dynamics of the system, we tried to emphasize that this mathematical model could be further used to examine which particular experimental treatments are more likely to reduce the size of the tumor.

As previously mentioned, the bi-stability phenomenon was possible only under the assumption that there is a continuous source of effector cells that can kill the tumor (i.e., $i_{nl} \neq 0$). This assumption might not be very realistic, since the effectors are usually eliminated from the blood following infection clearance. This suggests that unless there is another immunological mechanism that leads to the long-time presence of effector cells, the bi-stable behavior between a tumor-free and a tumor-present state might not be very relevant from an experimental perspective.

The multi-instability phenomenon that leads to the elimination of tumor cells was associated here with long-time persistence of the vesicular stomatitis virus (VSV) (i.e., a low ω_v). In general, this virus is neuro-toxic for mice (but not humans). However, since neuro-virulence could be attenuated through molecular manipulations (Egan et al. 2004; Cooper et al. 2008), this prolonged virus persistence should not be of major concern. A more serious concern is a possible feedback loop caused by the VSV itself, which can limit its persistence. In particular, the oncolytic virus can stop the intra-tumor blood flow and kill the uninfected tumor cells (Breitbart et al. 2007). This, in turn, can limit the spread and the persistence of the virus (since the virus replicates only inside the tumor cells).

Another shortcoming of VSV is its basic reproduction ratio, which is usually less than one ($R_0 < 1$) (Lord and Tabachnick 2002). Hence, the effective reproduction

number (R_c^o) is also less than one. Our results suggest that using a different oncolytic virus (with a better half-life or a better replication rate) could improve the treatment.

Mathematical Implications The investigation of these two phenomena, multi-stability and multi-instability, was possible because of the decoupling of the anti-tumor immune response from the anti-tumor viral response. We suspect that other mathematical models that show similar decoupling mechanisms would exhibit similar behaviors.

In general, a multi-instability phenomenon observed in a tumor-immune-virus model does not necessarily mean that the tumor will be eliminated. The existence of steady states that are simultaneously unstable could cause, for example, chaotic behavior (as observed in some epidemiological models Billings and Schwartz 2002, or delayed models for virus-immune interactions Canabarro et al. 2004). Since model (4) has a very large parameter space, it might be possible to observe chaotic behavior in a different region of this space. However, our goal was not to investigate the entire parameter space. We only wished to suggest a mechanism, namely the homoclinic bifurcation caused by the multi-instability phenomenon, that could lead to tumor elimination. In addition, we showed that a thorough investigation of the global behavior of the system is absolutely necessary if we want to understand the effects of the non-linear interactions on the outcome of the treatment.

The current model can be simplified by ignoring the effect of the vaccine virus (Ad), and/or by reducing the number (types) of effector cells that we model (y_{ep} and y_{ei}). We are currently working with a simplified 1-compartment model to understand the conditions that cause the homoclinic bifurcation and the possibility of having additional chaotic behavior. A detailed investigation of the cascade of complex bifurcations shown by the simplified model (which includes also chaotic patterns following period-doubling bifurcations) will be presented in a forthcoming paper.

Acknowledgements This work was supported by the Terry Fox New Frontiers Program Project Grant #018005. We acknowledge fruitful discussions with Yonghong Wan and Brian D. Lichty.

Appendix A

Stability of TO Steady State In the following, we will briefly discuss the stability of the TO steady state. The Jacobian matrix associated with system (4) has seven eigenvalues. The first three eigenvalues are easy to calculate (they are the only non-zero terms on three specific rows and columns in the Jacobian matrix):

$$\lambda_1 = i_c - d_c, \quad \lambda_2 = -\omega_a, \quad \lambda_3 = -d_1 - m_{1p}. \quad (24)$$

Since $i_c < d_c$ and all model parameters are positive (see Table 1), these three eigenvalues are always negative.

The next two eigenvalues are the solutions of the quadratic equation

$$-\lambda^2 + (a_{21} - Ea_{26})\lambda + \delta ba_{26} + Ea_{26}a_{21} = 0, \quad (25)$$

where

$$a_{21} = -\delta - d_i \frac{y_{ep}^{*,1,2}}{h_{ep} + y_{ep}^{*,1,2}}, \tag{26a}$$

$$a_{26} = d_v \frac{x_u^{*,1,2}}{h_u + x_u^{*,1,2}}, \tag{26b}$$

$$E = \frac{\delta b}{R_e^o(\delta + d_i \frac{y_{ep}^{*,1,2}}{h_{ep} + y_{ep}^{*,1,2}})}. \tag{26c}$$

The two eigenvalues that satisfy (25) are

$$\lambda_{4,5} = -\frac{1}{2}(Ea_{26} - a_{21}) \mp \frac{1}{2}\sqrt{(Ea_{26} - a_{21})^2 + 4a_{26}(\delta b + a_{21}E)}. \tag{27}$$

Note that $Ea_{26} - a_{21} > 0$, and hence the sign of $\lambda_{4,5}$ is given by

$$\delta b + a_{21}E = \delta b \frac{(R_e^o - 1)}{R_e^o}. \tag{28}$$

If $R_e^o < 1$, then both $\lambda_{4,5} < 0$. If $R_e^o > 1$, then $\lambda_4 < 0$ and $\lambda_5 > 0$ (and hence the steady state TO is unstable). We remark here that it is not possible for $\lambda_{4,5}$ to have complex values:

$$(Ea_{26} - a_{21})^2 + 4a_{26}(\delta b + a_{21}E) = (Ea_{26} + a_{21})^2 + 4\delta ba_{26} > 0. \tag{29}$$

Finally, the last two eigenvalues, $\lambda_{6,7}$, satisfy equation

$$\lambda^2 - (a_{11} + a_{55})\lambda + a_{11}a_{55} + a_{15}d_t y_{ep}^{*,1,2} = 0, \tag{30}$$

where

$$a_{11} = r - 2rkx_u^{*,1,2} - d_u \frac{y_{ep}^{*,1,2}}{h_{ep} + y_{ep}^{*,1,2}} = -rkx_u^{*,1,2}, \tag{31a}$$

$$a_{15} = -d_u \frac{x_u^{*,1,2}h_{ep}}{(h_{ep} + y_{ep}^{*,1,2})^2}, \tag{31b}$$

$$a_{55} = -d_p - d_t x_u^{*,1,2} - m_{p1}. \tag{31c}$$

The two eigenvalues satisfying (30) are

$$\lambda_{6,7} = \frac{1}{2}(a_{11} + a_{55}) \pm \frac{1}{2}\sqrt{(a_{11} + a_{55})^2 - 4(a_{11}a_{55} + a_{15}d_t y_{ep}^{*,1,2})}. \tag{32}$$

Note that $a_{11} + a_{55} < 0$, and hence the sign of $\lambda_{6,7}$ is given by

$$a_{11}a_{55} + a_{15}d_t y_{ep}^{*,1,2} = \frac{x_u^{*,1,2}(d_p + d_t x_u^{*,1,2} + m_{pl})}{m_{lp} i_{nl}} \left(r k m_{lp} i_{nl} - d_u d_t h_{ep}(d_l + m_{lp}) \left(\frac{y_{ep}^{*,1,2}}{h_{ep} + y_{ep}^{*,1,2}} \right)^2 \right). \tag{33}$$

When

$$\left(\frac{y_{ep}^{*,1,2}}{h_{ep} + y_{ep}^{*,1,2}} \right)^2 < \frac{r k m_{lp} i_{nl}}{d_u d_l h_{ep}(d_l + m_{lp})}, \tag{34}$$

both $\lambda_{6,7} < 0$. Otherwise, $\lambda_6 < 0$ and $\lambda_7 > 0$, which makes the TO steady state unstable. We also remark that neither λ_6 nor λ_7 can take complex values, since $a_{15} < 0$, and thus

$$(a_{11} + a_{55})^2 - 4(a_{11}a_{55} + a_{15}d_t y_{ep}^{*,1,2}) = (a_{11} - a_{55})^2 - 4a_{15}d_t y_{ep}^{*,1,2} > 0. \tag{35}$$

Therefore, the equilibrium points are either stable nodes or unstable saddle points. This completes the proof of Lemma 2.

Existence Conditions for the TV Steady State The TV steady state is defined by the condition $R_e^v = 1$. In this case, the tumor TV state $x_u^{*,v}$ satisfies the implicit equation

$$x_u^{*,v,1,2} = \frac{(D - r k h_u) \mp \sqrt{(D - r k h_u)^2 + 4r k (h_u D - d_u v^*)}}{2r k}, \tag{36}$$

with

$$D = r - \frac{d_u y_{ep}^{*,v}}{h_{ep} + y_{ep}^{*,v}} - r k \frac{\omega_v v^*}{\delta b}. \tag{37}$$

If the TF state is stable (i.e., inequality (20) is satisfied), then $D < 0$ and the TV state does not exist. This TV state exists when both $R_e^v = 1$ and at least one of the following inequalities are satisfied:

$$r > \frac{d_u y_{ep}^{*,v}}{h_{ep} + y_{ep}^{*,v}} + r k \frac{\omega_v v^*}{\delta b} + r k h_u \quad \text{and} \quad (D + r k h_u)^2 > 4r k d_u v^*, \tag{38}$$

or

$$r > \frac{d_u y_{ep}^{*,v}}{h_{ep} + y_{ep}^{*,v}} + r k \frac{\omega_v v^*}{\delta b} + \frac{d_u v^*}{h_u}. \tag{39}$$

Appendix B

The parameter values used for the numerical simulations presented in this article are described in Table 1. Table 2 summarizes the variables in model (4).

Table 1 Parameter values used for numerical simulations of model (4). Some of the values are taken from the literature (see references below). The other values were chosen according to our best fit of available tumor, virus and immune data (see Bridle et al. 2010)

Parameter	Value	Units	Description & Reference
r	0.927	days ⁻¹	proliferation rate for tumor cells (Bridle et al. 2010)
k	5.5×10^{-9}	cells ⁻¹	k^{-1} = carrying capacity for the tumor cells
d_v	0.038	(cells)(PFU/ μ) ⁻¹ (days) ⁻¹	infection rate of tumor cells with the VSV
d_u	1.8	days ⁻¹	lysis rate of uninfected tumor cells by the immune cells (assumed similar to d_t)
h_u	1	cells	half-saturation constant for the tumor cells infected with the VSV
h_{ep}	40	cells	half-saturation constant for the effector cells that support half the maximum killing rate
h_v	10^{-3} - 10^4	PFU/ μ l	half-saturation constant of VSV antigens that induce half the maximum proliferation rate of immune cells
h_a	10^{-3} - 10^4	PFU/ μ l	half-saturation constant of Ad antigens that induce half the maximum proliferation rate of immune cells
δ	1	days ⁻¹	rate at which the VSV kills the tumor cells
d_i	1.8	days ⁻¹	lysis rate of infected tumor cells by the immune cells (Kündig et al. 1996)
i_c	3×10^{-9}	days ⁻¹	proliferation rate of memory cells in the absence of any stimuli
p_c^a	0.09	days ⁻¹	proliferation rate of memory cells in response to Ad antigens
p_c^v	0.09-0.1	days ⁻¹	proliferation rate of memory cells in response to VSV antigens (Bridle et al. 2010)
m_{pl}	10^{-5} - 10^{-2}	days ⁻¹	migration rate of effector and effector-memory cells from the periphery to the lymphoid compartment (de Boer et al. 2001)
r_{cl}	16.6	days ⁻¹	rate at which memory cells become effector cells following secondary infection
d_c	0.028	cells ⁻¹	death rate of memory cells
i_c	10^{-6} - 10^{-5}	(days ⁻¹)(PFU/ μ) ⁻¹	rate of memory cells reduction following VSV-induced lymphopenia (Bridle et al. 2010)
i_{nl}	0.6	(cells)(days) ⁻¹	flux rate at which the naive cells become effector cells following long-term antigen persistence
i_{nc}	0-0.6	(cells)(days) ⁻¹	flux rate at which the naive cells become memory cells following long-term antigen persistence
p_c^a	0.6	days ⁻¹	proliferation rate of effector and effector-memory cells in response to Ad antigens
p_c^v	0.6-2.5	days ⁻¹	proliferation rate of effector and effector-memory cells in response to VSV antigens (Bridle et al. 2010)
d_l	0.133	days ⁻¹	death rate of effector cells in the lymphoid compartment (Bridle et al. 2010)

Table 1 (Continued)

Parameter	Value	Units	Description & Reference
m_{lp}	0.34	days ⁻¹	migration rate of effector and effector-memory cells from the lymph nodes to periphery
l_1	10^{-7} – 2×10^{-5}	(days ⁻¹)(PFU/ μ) ⁻¹	rate of memory cells reduction following VSV-induced lymphopenia (Bridle et al. 2010)
d_p	0.133	days ⁻¹	death rate of effector cells in the periphery (Bridle et al. 2010)
d_t	3×10^{-10}	(cell) ⁻¹ (days) ⁻¹	inactivation rate of immune effector cells by the tumor cells
ω_v	13–50	days ⁻¹	decay rate for the concentration of VSV particles/antigen
ω_a	2.6	days ⁻¹	decay rate for the concentration of Ad particles/antigen
b	1000	(PFU/ μ)(cell) ⁻¹	number of virus particles released from an infected cell, capable of forming plaques
q	2.2	days ⁻¹	the decay rate of the VSV-induced lymphopenia (Schattnner et al. 1983)
g_v	1	(PFU/ μ) ⁻¹	g_v^{-1} = concentration of VSV antigens at half maximum (scaled value)
k_c	9×10^{-7}	cells ⁻¹	k_c^{-1} = carrying capacity for the memory cells (due to competition for space)
k_e	9×10^{-7}	cells ⁻¹	k_e^{-1} = carrying capacity for the effector cells (as a result of auto-inhibition)

Table 2 State variables used in model (4)

State variables	Meaning
x_u	Cancer cells: uninfected
x_i	Cancer cells: infected
y_{cm}	Immune cells: central memory cells
y_{el}	Immune cells: effector cells in the lymphoid compartment
y_{ep}	Immune cells: effector cells in the peripheral compartment
v_v	Virus particles: replicating (oncolytic) Vesicular Stomatitis Virus
v_a	Virus particles: non-replicating Adenovirus

References

- Alemanly, R., Suzuki, K., & Curiel, D. T. (2000). Blood clearance rates of adenovirus type 5 in mice. *J. Gen. Virol.*, *81*, 2605–2609.
- Angeli, D., Ferrell, J. E., & Sontag, E. D. (2004). Detection of multistability, bifurcations, and hysteresis in a large class of biological positive-feedback systems. *Proc. Natl. Acad. Sci. USA*, *101*(7), 1822–1827.
- Araujo, R. P., & McElwain, D. L. S. (2004). A history of the study of solid tumor growth: the contribution of mathematical modeling. *Bull. Math. Biol.*, *66*, 1039–1091.
- Badovinac, V. P., Tvinnereim, A. R., & Harty, J. T. (2000). Regulation of antigen-specific CD8⁺ T cell homeostasis by perforin and Interferon- γ . *Science*, *290*(5495), 1354–1357.
- Bahl, K., Kim, S.-K., Calcagno, C., Ghersi, D., Puzone, R., Celada, F., Selin, L. K., & Welsh, R. M. (2006). IFN-induced attrition of CD8 T cells in the presence or absence of cognate antigen during the early stages of viral infection. *J. Immunol.*, *176*, 4284–4295.
- Bajzer, Z., Carr, T., Josić, K., Russell, S. J., & Dingli, D. (2008). Modeling of cancer virotherapy with recombinant measles viruses. *J. Theor. Biol.*, *252*, 109–122.
- Biesecker, M., Kimn, J.-H., Lu, H., Dingli, D., & Bajzer, Z. (2010). Optimization of virotherapy for cancer. *Bull. Math. Biol.*, *72*, 469–489.
- Billings, L., & Schwartz, I. B. (2002). Exciting chaos with noise: unexpected dynamics in epidemic outbreaks. *J. Math. Biol.*, *44*(1), 31–48.
- Blohm, U., Pothhoff, D., van der Kogel, A. J., & Pircher, H. (2006). Solid tumors “melt” from the inside after successful CD8 T cell attack. *Eur. J. Immunol.*, *36*(2), 468–477.
- Bluming, A. Z., & Ziegler, J. L. (1971). Regression of Burkitt’s lymphoma in association with measles infection. *Lancet*, *2*(7715), 105–106.
- Breitbach, C. J., Paterson, J. M., Lemay, C. G., Falls, T. J., McGuire, A., Parato, K. A., Stojdl, D. F., Daneshmand, M., Speth, K., Kirn, D., McCart, J. A., Atkins, H., & Bell, J. C. (2007). Targeted inflammation during oncolytic virus therapy severely compromises tumor blood flow. *Molec. Ther.*, *15*(9), 1686–1693.
- Bridle, B. W., Boudreau, J. E., Lichty, B. D., Brunellière, J., Stephenson, K., Koshy, S., Bramson, J. L., & Wan, Y. (2009). Vesicular stomatitis virus as a novel cancer vaccine vector to prime antitumor immunity amenable to rapid boosting with adenovirus. *Molec. Ther.*, *17*(10), 1814–1821.
- Bridle, B. W., Stephenson, K. B., Boudreau, J. E., Koshy, S., Kazhdan, N., Pullenayegum, E., Brunellière, J., Bramson, J. L., Lichty, B. D., & Wan, Y. (2010). Potentiating cancer immunotherapy using an oncolytic virus. *Molec. Ther.*, *18*(8), 1430–1439.
- Brunner, K. T., Hures, D., McCluskey, R. T., & Benacerraf, B. (1960). Blood clearance rates of P₃₂-labeled vesicular stomatitis and Newcastle disease viruses by the reticuloendothelial system in mice. *J. Immunol.*, *85*, 99–105.
- Buhl, J., Sumpter, D. J. T., Couzin, I. D., Hale, J. J., Despland, E., Miller, E. R., & Simpson, S. J. (2006). From disorder to order in marching locusts. *Science*, *312*(5778), 1402–1406.
- Bunimovich-Mendrazitsky, S., Shochat, E., & Stone, L. (2007). Mathematical model of BCG immunotherapy in superficial bladder cancer. *Bull. Math. Biol.*, *69*, 1847–1870.
- Byrne, H. M., Cox, S. M., & Kelly, C. E. (2004). Macrophage-tumor interactions: In vivo dynamics. *Discrete Contin. Dyn. Syst., Ser. B*, *4*(1), 81–98.

- Canabarro, A. A., Gléria, I. M., & Lyra, M. L. (2004). Periodic solutions and chaos in a non-linear model for the delayed cellular immune response. *Physica A*, *342*, 234–241.
- Cappuccio, A., Castiglione, F., & Piccoli, B. (2007). Determination of the optimal therapeutic protocols in cancer immunotherapy. *Math. Biosci.*, *209*(1), 1–13.
- Chang, H. H., Oh, P. Y., Ingber, D. E., & Huang, S. (2006). Multistable and multistep dynamics in neurophil differentiation. *BMC Cell Biol.*, *7*, 11.
- Choi, B. K., Kim, Y. H., Kan, W. J., Lee, S. K., Kim, K. H., Shin, S. M., Yokoyama, W. M., Kim, T. Y., & Kwon, B. S. (2007). Mechanisms involved in synergistic anticancer immunity of anti-4-1BB and anti-CD4 therapy. *Cancer Res.*, *67*(18), 8891–8899.
- Choisy, M., Guégan, J.-F., & Rohani, P. (2006). Dynamics of infectious diseases and pulse vaccination: teasing apart the embedded resonance effects. *Physica D*, *223*, 26–35.
- Cooper, D., Wright, K. J., Calderon, P. C., Guo, M., Nasar, F., Johnson, J. E., Coleman, J. W., Lee, M., Kotash, C., Yurgeloni, I., Natuk, R. J., Hendry, R. M., Udem, S. A., & Clarke, D. K. (2008). Attenuation of recombinant vesicular stomatitis virus-human immunodeficiency virus type 1 vaccine vectors by gene translocation and G gene truncation reduces neurovirulence and enhances immunogenicity in mice. *J. Virol.*, *82*(1), 207–219.
- Curran, M. A., Montalvo, W., Yagita, H., & Allison, J. P. (2010). PD-1 and CTLA-4 combination blockade expands infiltrating T cells and reduces regulatory T and myeloid cells within B16 melanoma tumors. *Proc. Natl. Acad. Sci. USA*, *107*(9), 4275–4280.
- de Boer, R. J., Oprea, M., Antia, R., Murali-Krishna, K., Ahmed, R., & Perelson, A. S. (2001). Recruitment times, proliferation, and apoptosis rates during the CD8⁺ T-cell response to lymphocytic choriomeningitis virus. *J. Virol.*, *75*(22), 10663–10669.
- Diaz, R. M., Galivo, F., Kottke, T., Wongthida, P., Qiao, J., Thompson, J., Valdes, M., Barber, G., & Vile, R. G. (2007). Oncolytic immunotherapy for melanoma using vesicular stomatitis virus. *Cancer Res.*, *67*(6), 2840–2848.
- Dingli, D., Offord, C., Myers, R., Peng, K.-W., Carr, T. W., Josic, K., Russell, S. J., & Bajzer, Z. (2009). Dynamics of multiple myeloma tumor therapy with a recombinant measles virus. *Cancer Gene Ther.*, *16*(12), 873–882.
- Dock, G. (1904). Rabies virus vaccination in a patient with cervical carcinoma. *Am. J. Med. Sci.*, *127*, 563.
- Earn, D. J. D., Rohani, P., Bolker, B. M., & Grenfell, B. T. (2000). A simple model for complex dynamical transitions in epidemics. *Science*, *287*(5453), 667–670.
- Eftimie, R., Bramson, J. L., & Earn, D. J. D. (2010). Interactions between the immune system and cancer: a brief review of non-spatial mathematical models. *Bull. Math. Biol.*, *73*(1), 2–32.
- Egan, M. A., Chong, S. Y., Rose, N. F., Megati, S., Lopez, K. J., Schadeck, E. B., Johnson, J. E., Masood, A., Piacente, P., Duilhet, R. E., Barras, P. W., Hasselschwert, D. L., Reilly, P., Mishkin, E. M., Montefiori, D. C., Lewis, M. G., Clarke, D. K., Hendrix, R. M., Marx, P. A., Eldridge, J. H., Udem, S. A., Israel, Z. R., & Rose, J. K. (2004). Immunogenicity of attenuated vesicular stomatitis virus vectors expressing HIV type 1 Env and SIV Gag proteins: comparison of intranasal and intramuscular vaccination routes. *AIDS Res. Hum. Retrovir. B*, *20*(9), 989–1004.
- Eißing, T., Conzelmann, H., Gilles, E., Allgöwer, F., Bullinger, E., & Scheurich, P. (2004). Bistability analysis of a caspase activation model for receptor-induced apoptosis. *J. Biol. Chem.*, *279*, 36892–36897.
- Ferreira, S. C., Martins, M. L., & Vilela, M. J. (2005). Fighting cancers with viruses. *Physica A*, *345*(3–4), 591–602.
- Fiasconaro, A., Ochab-Marcinek, A., Spagnolo, B., & Gudowska-Nowak, E. (2008). Monitoring noise-resonant effects in cancer growth influenced by external fluctuations and periodic treatment. *Eur. Phys. J. B*, *65*, 435–442.
- Finn, J. D., Bassett, J., Millar, J. B., Grinshtein, N., Yang, T. C., Parsons, R., Eveleigh, C., Wan, Y., Parks, R. J., & Bramson, J. L. (2009). Persistence of transgene expression influences CD8⁺ T-cell expansion and maintenance following immunization with recombinant adenovirus. *J. Virol.*, *83*(23), 12027–12036.
- Friedman, A., Tian, J. P., Fulci, G., Chiocca, E. A., & Wang, J. (2006). Glioma virotherapy: effects of innate immune suppression and increased viral replication capacity. *Cancer Res.*, *66*(4), 2314–2319.
- Hansen, R. M., & Libnoch, J. A. (1978). Remission of chronic lymphocytic leukemia after smallpox vaccination. *Arch. Intern. Med.*, *138*, 1137–1138.
- Kaech, S. M., Wherry, E. J., & Ahmed, R. (2002). Effector and memory T-cell differentiation: implications for vaccine development. *Nat. Rev. Immunol.*, *2*, 251–262.
- Kirschner, D., & Panetta, J. C. (1998). Modeling immunotherapy of the tumor-immune interaction. *J. Math. Biol.*, *37*, 235–252.

- Kündig, T. M., Bachmann, M. F., Oehen, S., Hoffmann, U. W., Simard, J. J. L., Kalberer, C. P., Pircher, H., Ohashi, P. S., Hengartner, H., & Zinkernagel, R. F. (1996). On the role of antigen maintaining cytotoxic T-cell memory. *Proc. Natl. Acad. Sci. USA*, *93*, 9716–9723.
- Lefever, R., & Horsthemke, W. (1979). Bistability in fluctuating environments. Implications in tumor immunology. *Bull. Math. Biol.*, *41*, 469–490.
- Lejeune, O., Chaplain, M. A. J., & El Akili, I. (2008). Oscillations and bistability in the dynamics of cytotoxic reactions mediated by the response of immune cells to solid tumors. *Math. Comput. Model.*, *47*, 649–662.
- Lord, C. C., & Tabachnick, W. J. (2002). Influence of nonsystemic transmission on the epidemiology of insect borne arboviruses: a case study of vesicular stomatitis epidemiology in the Western United States. *J. Med. Entomol.*, *39*(3), 417–426.
- Marsden, V. S., Kappler, J. W., & Marrack, P. C. (2006). Homeostasis of the memory T cell pool. *Int. Arch. Allergy Immunol.*, *139*, 63–74.
- Mullen, J. T., & Tanabe, K. K. (2002). Viral oncolysis. *Oncologist*, *7*, 106–119.
- Munks, M. W., Mourich, D. V., Mittler, R. S., Weinberg, A. D., & Hill, A. B. (2004). 4-1BB and OX40 stimulation enhance CD8 and CD4 T-cell responses to a DNA prime, poxvirus boost vaccine. *Immunology*, *112*, 559–566.
- Nowak, M., & May, R. (2000). *Virus dynamics: mathematical principles of immunology and virology*. London: Oxford University Press.
- Paiva, L. R., Binny, C., Ferreira, S. C. Jr., & Martins, M. L. (2009). A multiscale mathematical model for oncolytic virotherapy. *Cancer Res.*, *69*(3), 1205–1211.
- Perko, L. (2000). *Differential equations and dynamical systems*. New York: Springer.
- Pomeroy, J. R. (2008). Uncovering mechanisms of bistability in biological systems. *Curr. Opin. Biotechnol.*, *19*(4), 381–388.
- Reth, M., & Brummer, T. (2004). Feedback regulation of lymphocyte signaling. *Nat. Rev. Immunol.*, *4*, 269–277.
- Sallusto, F., Geginat, J., & Lanzavecchia, A. (2004). Central memory and effector memory T cell subsets: function, generation, and maintenance. *Annu. Rev. Immunol.*, *22*, 745–763.
- Schattner, A., Meshorer, A., & Wallach, D. (1983). Involvement of interferon in virus-induced lymphopenia. *Cell. Immunol.*, *79*, 11–25.
- Schwartz, I. B., & Carr, T. W. (1999). Bi-instability as a precursor to global mixed-mode chaos. *Phys. Rev. E*, *59*(6), 6658–6661.
- Schwartz, I. B., & Smith, H. L. (1983). Infinite subharmonic bifurcation in an SEIR model. *J. Math. Biol.*, *18*, 233–253.
- Silva, N. D., Atkins, H., Kirn, D. H., Bell, J. C., & Breitbach, C. J. (2010). Double trouble for tumours: Exploiting the tumour microenvironment to enhance anticancer effect of oncolytic viruses. *Cytokine Growth Factor Rev.*, *21*(2–3), 135–141.
- Thompson, J. M. T., Stewart, H. B., & Ueda, Y. (1994). Safe, explosive, and dangerous bifurcations in dissipative dynamical systems. *Phys. Rev. E*, *49*, 1019–1027.
- Turner, D. L., Cauley, L. S., Khanna, K. M., & Lefrançois, L. (2007). Persistent antigen presentation after acute vesicular stomatitis virus infection. *J. Virol.*, *81*(4), 2039–2046.
- Wein, L. M., Wu, J. T., & Kirn, D. H. (2003). Validation and analysis of a mathematical model of a replication-competent oncolytic virus for cancer treatment: implications for virus design and delivery. *Cancer Res.*, *63*, 1317–1324.
- Wherry, E. J., Teichgräber, V., Becker, T. C., Masopust, D., Kaech, S. M., Antia, R., von Andrian, U. H., & Ahmed, R. (2003). Lineage relationship and protective immunity of memory CD8 T cell subsets. *Nat. Immunol.*, *4*(3), 225–234.
- Wodarz, D. (2001). Viruses as antitumor weapons: defining conditions for tumor remission. *Cancer Res.*, *61*, 3501–3507.
- Wodarz, D., & Komarova, N. (2009). Towards predictive computational models of oncolytic virus therapy: basis for experimental validation and model selection. *PLoS ONE*, *4*(1), e4271.
- Wu, J. T., Kirn, D. H., & Wein, L. M. (2004). Analysis of a three-way race between tumor growth, a replication-competent virus and an immune response. *Bull. Math. Biol.*, *66*(4), 605–625.